ELSEVIER

Lithos 36 (1995) 289–303

LITHOS

Revealing hidden structures: The application of cathodoluminescence and back-scattered electron imaging to dating zircons from lower crustal xenoliths

J.M. Hanchar [a,*], R.L. Rudnick [b,c]

[a] *Department of Earth and Environmental Sciences, Rensselaer Polytechnic Institute, Troy, NY 12180, USA*

[b] *Research School of Earth Sciences, The Australian National University, Canberra, ACT 2601, Australia*

[c] *Now at: Department of Earth and Planetary Sciences, Harvard University, 20 Oxford St., Cambridge, MA 02138, USA*

Received 5 December 1994; accepted 5 May 1995

Abstract

The use of cathodoluminescence (CL) and/or back-scattered electron (BSE) imaging techniques with in situ ion probe analyses of zircons can help unravel complex crustal histories of metamorphic rocks that otherwise might remain elusive. Using these techniques we have imaged zircons from three lower crustal xenolith suites that have previously been dated by SHRIMP (sensitive high-resolution ion microprobe). In all three cases, the zircons are featureless in transmitted light but CL and BSE reveal internal structures that correlate with distinct growth events. Generally, CL and BSE images reveal similar structures, with CL showing finer detail. Neither imaging technique is capable of delineating all growth features in every sample and the best results are obtained using a combination of the two techniques. Igneous cores in zircons commonly emit a different color CL emission. In many cases zoning in the cores is truncated, indicating that the zircons either spent time in the supracrustal environment after their initial crystallization and prior to the granulite facies event(s) or that part of the core zircon was resorbed during the subsequent metamorphic event. Metamorphic rims, when present, are commonly 10 to 30 μm thick, and are nearly always unzoned and featureless.

Igneous cores and metamorphic overgrowths commonly have distinctive CL emission spectra and trace element concentrations. However, the CL spectra can only be used to qualify chemical differences, as a linear relationship has not been shown to exist between CL intensity and trace element concentration in natural zircons. In many cases the Hf, Y, P, U and the heavy rare-earth elements (HREEs) concentrations can be correlated to igneous and metamorphic growth using a combination of CL and BSE imaging techniques and in situ trace element analyses with either the electron microprobe or PIXE (particle induced X-ray emission).

1. Introduction

Granulite facies xenoliths carried by recent alkali basalts and kimberlites provide one of the few avenues available for studying the mineralogy and composition of the present day lower continental crust. Determining when the xenoliths formed and when they experienced high-grade metamorphism is critical to placing the xenoliths into the geologic framework of a region and provides the most reliable information on when the lower crust formed.

A powerful tool for determining ages of high-grade rocks is single crystal U–Pb zircon geochronology (Krogh, 1993). This is due to the extreme incompati-

* Corresponding author.

SSDI 0024-4937(95)00022-4

bility of common Pb in zircon, and because zircon is capable of retaining radiogenic Pb during high temperature and pressure metamorphic events (e.g., Heaman and Parrish, 1991). In particular, ion microprobe dating of zircons from granulites has the potential to reveal the original crystallization age as well as the age of subsequent metamorphic events within a single rock (e.g., Black et al., 1984; Rudnick and Williams, 1987; Williams and Claesson, 1987).

In granulites having multiple zircon generations, individual zircon grains are commonly zoned. It is desirable to be able to delineate these zones as a guide to both ion probe and isotope dilution single crystal analyses. For granulites that have resided at the Earth's surface for hundreds of millions of years (most granulite facies terranes), this is generally possible due to the variable U contents in different zircon growth zones and the resulting metamictization from α-recoil decay. Etching a zircon (mounted in epoxy and polished to half its thickness) with HF acid serves to enhance these features when viewed with reflected light microscopy (Black et al., 1984). In contrast, most granulite facies xenoliths have been at the Earth's surface for considerably shorter periods of time [host lavas for most granulite xenoliths are Tertiary or younger (Rudnick, 1992)]. Radiation damage to the zircon structure appears to be annealed out in the hot lower crust, since these zircons show no visible metamictization either in plane-polarized light (PPL) or on acid-etched surfaces (e.g., Rudnick and Williams, 1987). Thus possible growth zones or inherited cores remain invisible.

Cathodoluminescence (CL) and back-scattered electron (BSE) imaging may provide the only way of delineating structure in annealed zircons. Previous studies have demonstrated that zoning is widespread in zircons and carries considerable information regarding the history of the zircon (e.g., Sommerauer, 1974, 1976; Miller et al., 1992; Paterson et al., 1992; Hanchar and Miller, 1993). In addition, preservation of zoning through multiple high-grade geologic events demonstrates that diffusion of the trace elements responsible for the zoning must be extremely slow (Cherniak et al., 1993).

In this paper we apply CL and BSE imaging techniques to zircons from lower crustal xenoliths that have been dated using the SHRIMP (sensitive high-resolution ion microprobe). These techniques reveal otherwise invisible structures that delineate different age events in zircons (e.g., inherited igneous cores preserving original, and in some cases subsequent, crystallization information, one or more metamorphic overgrowths) thus facilitating the interpretation of ion probe analyses. We demonstrate that no single imaging technique is capable of delineating all growth features in every example and that the best results are obtained using a combined approach of the two techniques.

2. Methods

The CL images presented in this paper were taken at Rensselaer Polytechnic Institute using a Premier American Technologies Corporation ELM-3R Luminoscope operating in regulated current mode at 12 kV and 0.5 mA. The film used to record the CL photomicrographs was Kodak Ektachrome 200 color slide film. Exposure times for the photomicrographs ranged from 60 to 180 s.

CL spectra were collected with an Acton Research ARC 150 Spectrograph (146 mm focal length) equipped with an 1800 groove/mm holographic grating coupled directly to an Olympus BH-2 microscope. The entrance slits were set at 25 μm, to give a spectral resolution of approximately 0.15 nm. The CL emission was detected using a Princeton Instruments TEA/CCD-576EMUV 576×384 charge-coupled device (CCD) detector cooled to -40°C with a Peltier thermoelectric cooler. The spectra were collected using Princeton Instruments, Inc., CSMA software interfaced to a Zenith 486-33 computer through an interface card, and further processed with Igor Pro by WaveMetrics, Inc. The spatial resolution of this system (i.e., the smallest region within in a crystal from which a CL spectra can be collected) is approximately 10 μm by 10 μm. The CL emission spectra are calibrated against known emission lines from Hg, Ar and Ne.

The BSE images were taken at Rensselaer Polytechnic Institute with a JEOL 733 Superprobe using a beam current of 50–200 nA and an accelerating voltage of 10–30 kV, depending on the zircon. The CL samples were uncoated and the BSE samples were carbon coated to a thickness of 100–200 Å depending on the zircon and the conductivity of the epoxy mount. The BSE images were recorded using Polaroid type 53 and 55 black and white film.

The electron microprobe analyses were performed on a JEOL 733 Superprobe using a current of 150 nA at an accelerating voltage of 20 kV. Collimators were used to reduce peak interferences and to maximize peak to background ratios. Long counting times (to 480 s) yielded analytical uncertainties (1 σ) in the range of 0.2% for Hf, and 5–15% for Y, P, U and the heavy rare-earth elements (HREEs). Matrix corrections were performed using standard ZAF techniques. Standards used include synthetic zircon for Si and Zr, Hf metal for Hf, synthetic xenotime for Y and P, synthetic UO_2 for U, and Drake and Weill (1972) glasses for the rare-earth elements (REEs).

3. The CL and BSE Imaging Techniques

The CL visible light emission observed in crustal zircons is attributed primarily to Dy^{3+} (e.g., Mariano, 1978, 1988, 1989; Marshall, 1988; Remond et al., 1990, 1992), although Tb^{3+} and Y^{3+} may also be CL emitters (e.g., Ohnenstetter et al., 1991; Yang et al., 1992). In our experience with zircons derived from crustal rocks, the CL emission is usually due to Dy^{3+}, with a secondary contribution from Tb^{3+}, although in many zircons there are also broad band "intrinsic" emissions in the blue and yellow regions of the visible spectrum with peaks from Dy^{3+} and in some cases Tb^{3+}, superimposed on top of the "intrinsic" band (Mariano, 1989; Hanchar et al., in prep.). Ohnenstetter et al. (1991) have suggested that the broad band blue CL emission may be defect related due to the presence of Y^{3+}, and that the broad band yellow CL emission may also be defect related due to the presence of Ti^{4+} or U^{4+}. It should be stressed, however, that Ohnenstetter et al. (1991) suggest that the presence of these elements could cause lattice defects that lead to what is known as "intrinsic" yellow and blue CL emission in zircon, and not that the presence of Y^{3+}, Ti^{4+} or U^{4+} cause the narrow band CL emission characteristic of the REEs.

BSE images reveal contrasts in average atomic number of a phase; the higher the number, the more electrons an area will "reflect" and the brighter it will appear. The element primarily responsible for these BSE variations in crustal zircons is Hf, with U having a secondary effect (Hanchar and Miller, 1993). In investigating zircons with these imaging techniques we have found that in many cases both techniques reveal the same features; however, usually the bright areas in CL are dark in BSE and vise versa, an observation also noted by Koschek (1993). Subtle features are often visible with one technique and not the other. We have found that CL is generally more useful than BSE in identifying different growth regions in zircons due to the greater range in intensity and the additional variable of color. In addition, different growth zones often have characteristic CL emission.

A drawback to CL, however, is that there is a size limitation to the zircons that can be imaged. This is due to a combination of factors: (1) A leaded glass shield is used to attenuate X-rays emitted from the sample. Most objectives with greater than 15× magnification do not allow for correction of this shield, thus the resulting high magnification CL images are distorted; (2) Most objectives greater than 15× do not have a long enough "working distance" (i.e., long enough to incorporate the leaded glass as well as the space required between the sample and the leaded glass for the electrons to pass and impinge upon the sample). Thus, it is difficult to image zircons smaller than approximately 60 μm. The ideal zircon size for CL imaging is around 100–150 mm or larger, with which a 15× objective and 5× photo eyepiece can be used for photomicrographs and CL spectroscopy. The photomicrographs in this paper were taken using a 10 or 15× objective and 3.3 or 5× photo eyepiece.

4. Samples

The zircons investigated in this study were originally extracted for SHRIMP analyses from granulite facies lower crustal xenoliths from the McBride province, Queensland, Australia (Rudnick and Taylor, 1987; Rudnick and Williams, 1987), La Olivina, Chihuahua, Mexico (Rudnick and Cameron, 1991; Cameron et al., 1992) and the Newer Basalts, Victoria, Australia (King et al., 1993). Table 1 lists the xenolith lithologies, inferred petrogenesis and results of previous SHRIMP investigations.

5. Results

5.1. The McBride province xenoliths

Zircons from six xenoliths from the McBride province were investigated for this study; all appear struc-

Table 1
Descriptions of xenoliths that have been dated by SHRIMP

Sample	Rock type	Petrogenesis[a]	U–Pb Zircon age (s)
	McBride Province, N. Queensland, Australia		
83-162	Felsic granulite	Metamorphosed dacite	200–300 Ma
83-160	Felsic granulite	Metamorphosed dacite	200–300 Ma
85-107	Mafic granulite	Cumulate from granitic magma	240–340 Ma
85-100	Mafic granulite	Metamorphosed basalt	250–400 Ma, 500–1140 Ma
83-157	Pelitic granulite	Metamorphosed sedimentary rock	250 Ma, 1570 Ma
83-159	Mafic granulite	Restite	260 Ma, 1520 Ma
	La Olivina, Mexico		
MN-20	Mafic granulite	Mafic cumulate	1 Ma
MN-40	Felsic granulite	Metamorphosed trachydacite	25–37 Ma, 200 Ma
MN-19	Intermed. gran.	Metamorphosed basaltic andesite	10–360 Ma
GNX-22	Pelitic granulite	Metamorphosed shale	15–900 Ma
GNX-20	Intermed. gran.	Metamorphosed trachyandesite	7–30 Ma, 1.1 Ga, 1.4 Ga
	Newer Basalts, Victoria, Australia		
84-400	Pelitic granulite	Metamorphosed shale	175 to ~1700 Ma

[a]Petrogeneses from Rudnick and Taylor (1987) for McBride xenoliths, Cameron et al. (1992) for La Olivina xenoliths. Petrogenesis of meta-igneous rocks based on IUGS classificiation of volcanic rocks (Le Bas and Streckeisen, 1991).

tureless in PPL or reflected light (Fig. 1a). The results for zircons from four of the xenoliths are discussed below. These zircons generally reveal no internal features in BSE, except for a rare core. In CL, however, these zircons reveal complex internal relations (Fig. 1). Although most of the zircons used in this study retain their original SHRIMP probe pits, the zircons from the McBride samples were re-polished after SHRIMP analyses so it is difficult to determine the exact analysis locations. The colors referred to herein are the colors emitted by CL.

Metaadamellite 83-162. The ion probe analyses for these zircons lie within error of concordia between 300 to 200 Ma (Rudnick and Williams, 1987). Although the zircons are completely transparent in PPL, possible core–rim relations were identified in about half the zircons by the presence of a concentric shell of CO_2-rich fluid inclusions (Rudnick and Williams, Fig. 2a). However, SHRIMP analyses were unable to distinguish age differences between cores and rims in all but 1 zircon (#16, which has a 50 Ma age difference between core and rim).

CL reveals three types of zircons in this mount: (1) Zircons with 30–60 μm cores that emit a bright green, and in some cases dull gray to black CL, surrounded by bright blue overgrowths (10–30 μm in thickness). These zircons tend to be the largest in the mount (Fig. 1c). (2) Zircons that are similar to the first type except that they emit green to gray CL throughout with no blue CL overgrowth. (3) Zircons that emit a blue CL emission, are essentially structureless, and do not contain cores (Fig. 1c). When present, the CO_2-rich fluid inclusions occur exclusively within the cores, which may explain why most zircons showed no age difference between core and rim as defined by the presence of the CO_2-rich fluid inclusions. We infer the green and dull gray black cores (as revealed by CL) to be inherited igneous cores, and the bright blue regions to be metamorphic overgrowths (see discussion section below).

Mafic cumulate 85-107. There are two morphological groups of the zircons in this xenolith: round clear zircons, and large, elongate, light-brown zircons (in PPL) (Rudnick and Williams, 1987). These zircons contain abundant inclusions of felsic glass, apatite, clinopyroxene, magnetite, ilmenite and pyrrhotite (Rudnick and Williams, 1987). All of the ion probe analyses in 85-107 fall within error of concordia and have $^{206}Pb/^{238}U$ ages between 240 and 340 Ma (Rudnick and Williams, 1987). Rudnick and Williams inferred the older ages to reflect the original crystallization event (i.e., igneous core ages) and the younger ages to reflect the granulite-facies metamorphism. In this and other McBride samples, it was not possible to date the granulite facies metamorphism precisely.

CL reveals a variety of internal structures in these zircons. In the elongate grains, the inclusions occur exclusively within igneous cores, which emit a dull green to gray CL and are surrounded by bright blue, and in some cases yellow, metamorphic overgrowths ~10–15 μm thick (Fig. 1d). These rims are significantly smaller than the spot size used during the SHRIMP work (i.e., 20–30 μm), so their ages cannot be determined from the present data set. Many zircons are fractured fragments of larger grains, with cores exposed at the edge of the grains, and there is a high degree of asymmetry in the core–rim relations (i.e., the

cores are variable in size and do not always occur in the center of the zircons). Not all of the cores contain melt inclusions and a few cores emit a yellow CL. There are also zircons that emit a yellow CL throughout, contain no inclusions, and do not have overgrowths. Also present are zircons that emit a blue CL throughout, similar in color to the metamorphic overgrowths.

The round, clear zircons also commonly have igneous cores (some with melt inclusions) and bright blue CL metamorphic overgrowths. Some of these zircons consist of fragments of inherited cores with no overgrowths, similar to the yellow zircons described above, and there are purely metamorphic zircons, with blue CL, with no cores. These two varieties of round zircons are indistinguishable in transmitted or reflected light.

Metasedimentary granulite 83-157. Two morphologies of zircon occur within this xenolith: (1) clear, rounded zircons and (2) pale yellow (in PPL, not CL), elongate zircons (Rudnick and Williams, 1987). The small, round zircons yield $^{206}Pb/^{238}U$ ages that fall within error of concordia at 250 ± 20 Ma. The elongate zircons fall within two age groups: all but one define a chord between 1570 ± 100 Ma and 225 ± 90 Ma. One zircon, however, has a 2060 Ma concordant core, and interior zone that is strongly discordant and an outer rim which is nearly concordant at 1580 Ma. We believe that this age distribution can, in part, be explained by the internal structures observed using CL.

Most of the clear, rounded zircons are glassy and featureless in CL with no obvious internal structure. These emit a bright blue, yellow or pink CL. However, some of the round zircons contain small cores with yellow to green CL and igneous growth zoning (e.g., Ono, 1976; Vocke and Hanson, 1981; Paterson et al., 1992; Hanchar and Miller, 1993). These are surrounded by 20 to 30 μm thick rims that display the same range of colors as the featureless zircons. When present, the cores are relatively small compared to the size of the overgrowth, creating a high probability that a random SHRIMP analysis would be located in an overgrowth region and not in the core. Additionally, many of the cores are located near the edge of the grain, not in the center. Both of these factors lead to the likelihood of a SHRIMP analysis spot in the center of the grain would hit an overgrowth rather than an old component. We suggest that this may explain the cluster of ages at 250 ± 20 Ma.

CL reveals extremely complex internal structures in the elongate zircons. These zircons generally contain cores (Fig. 1e and f), and many have metamorphic overgrowths similar in color to the round zircons but generally much thinner. Many of the elongate zircons do not have metamorphic rims, and we infer these to be zircon cores that were somehow isolated from the metamorphic event. Many of the elongate zircons, including those with and without metamorphic rims, contain multiple cores and clustering of cores surrounded by an outer core (synneusis). Many of the cores (as revealed by CL) contain igneous growth zoning (Fig. 1e and f).

For this population, the chord defined by Rudnick and Williams (1987) can be explained by Pb-loss and in some cases, the spot overlapping inherited igneous cores (1570 Ma) and metamorphic overgrowths (225 Ma). In the case of the 2060 Ma zircon, the analysis may have been performed on an inner core, and the "rim" analysis may actually have been performed on an outer core that grew during the 1570 Ma age event. Due to subsequent polishing of the SHRIMP mount, the analysis pits were removed, and it is impossible to tell. The elongate zircons exhibit a wide variety of core positions and sizes and many core–rim combinations are possible.

Many of the inner cores show paleofractures in CL (Fig. 1e), reflecting residence of the original zircon in a supracrustal environment before the next period of zircon growth (e.g., Hanchar and Miller, 1993). CL also reveals that many of the cores contain igneous growth zoning that is truncated at the boundary of the core, which in many cases are well rounded (Fig. 1f). Fracturing and rounding (revealed through CL and BSE) is common in zircons from sedimentary rocks and in modern sediments (Hanchar and Miller, 1993) and is consistent with the interpretation of this rock as a metasediment (Rudnick and Williams, 1987).

Mafic restite 83-159. Morphologically, these zircons are unlike those from 83-157 and the other McBride xenoliths; they are quite large, up to 300 μm, and clear in PPL. Recrystallized silicate melt inclusions are present in the cores of some zircons as well as acicular apatite (Rudnick and Williams, 1987, Fig. 2i). The SHRIMP U–Pb results define two age populations: (1) older zircons lie on a chord between ca. 1520 Ma and 260 Ma; most analyses are strongly discordant (Rudnick and Williams, 1987; (2) younger zircons scatter

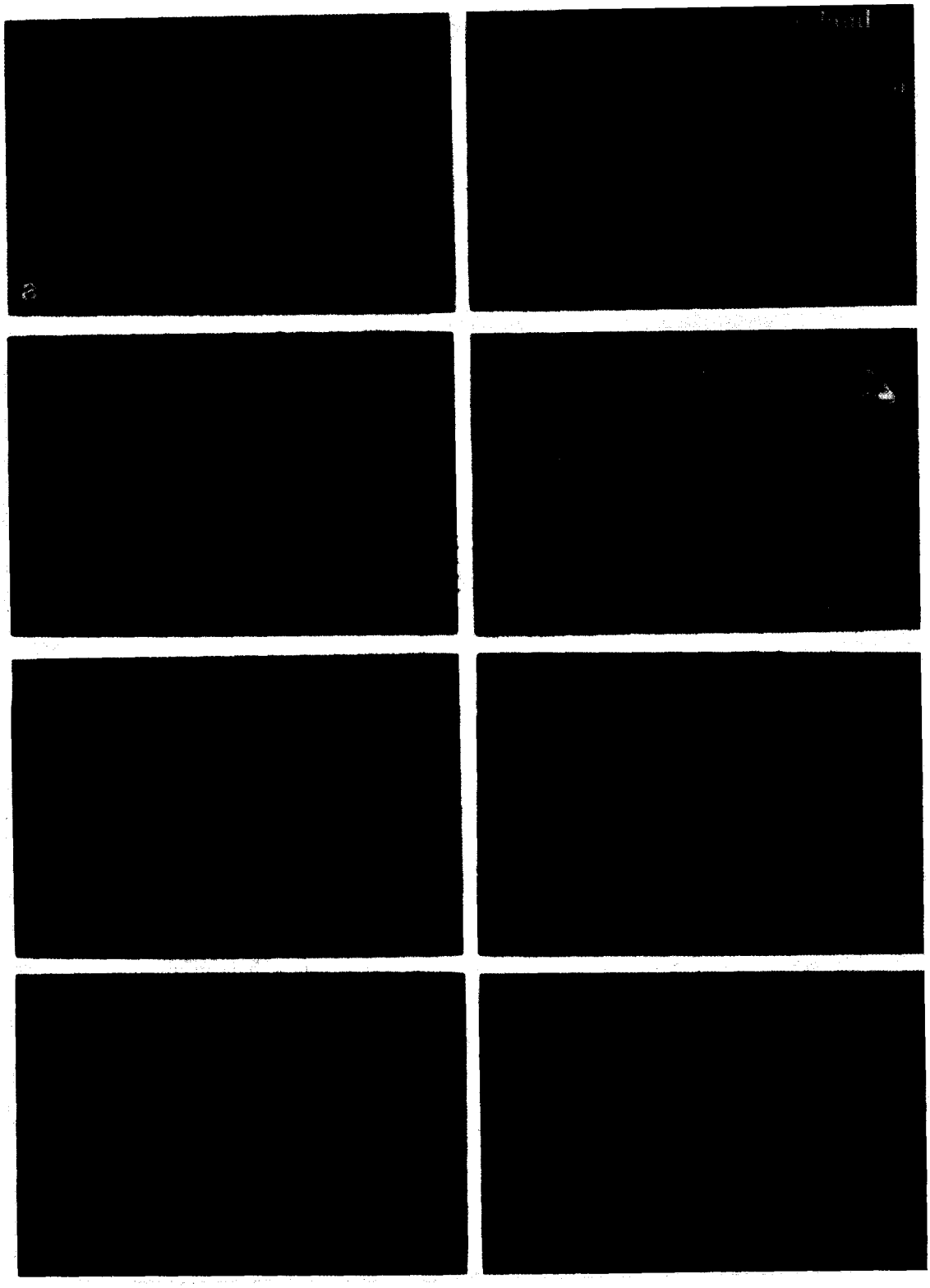

along concordia between 200 and 350 Ma, similar to zircons from other xenoliths in the McBride suite (fig. 4g of Rudnick and Williams, 1987). Rudnick and Williams interpreted these results, in conjunction with whole rock chemical data, to reflect zircon crystallization in an evolved igneous protolith around 1520 Ma ago followed by partial melting of the protolith in the late Paleozoic leaving a mafic, zircon-bearing residue which experienced a later Pb-loss event.

CL images reveal that some grains consist solely of metamorphic zircon with no core, whereas others consist of igneous grains with no overgrowths. Most, however, consist of an igneous core (some with multiple growth zones) and blue overgrowth (Fig 1b). The color of the CL in the overgrowth of Fig. 1b is similar to that of the metamorphic rims seen in other zircons from this sample (e.g., Fig. 1g), however, the trace element composition of this overgrowth is unlike that of metamorphic rims (see discussion section below). Thus in this sample, blue overgrowths may have either an igneous or metamorphic origin, as distinguished by the trace element systematics discussed below. Subtle color variations between different blue overgrowths may delineate igneous versus metamorphic zircon.

An example of a metamorphic overgrowth is shown in Fig. 1g. This zircon has a greenish-yellow core with igneous growth zoning surrounded by a relatively thick unzoned blue CL metamorphic overgrowth, typical of some of the zircons from this xenolith (the core is also observed in BSE, but the zoning is not). The trace element composition of the core and overgrowth from the zircon in Fig. 1g are distinct (see discussion section below). Most of the metamorphic overgrowths are 15 to 25 μm thick, but some are up to 80 to 100 μm thick.

Igneous growth zoning in the cores is commonly truncated, and in this regard these zircons are similar to those from 83-157 (Fig. 1h). This may suggest that these zircons spent time in the supracrustal environment after their initial igneous crystallization and prior to the granulite facies metamorphism. Alternatively, these features may also be produced by resorption of zircon in an igneous melt that is undersaturated with respect to zircon. The trace element compositions of the rims on the zircons in Fig 1h are similar to the rims in Fig. 1b, however, they are unlike the clearly identified metamorphic rims in Fig. 1g. Mineral (i.e., apatite, sulfides and pargasitic amphibole) and melt inclusions in these zircons reported by Rudnick and Williams (1987) are restricted to the igneous cores.

The structures revealed by CL and BSE imaging of these zircons, the results of the SHRIMP analyses as well as the zircon trace element systematics lead to the following geological history for this sample. Crystallization of an evolved igneous protolith at ~ 1520 Ma gave rise to the yellow-green igneous cores. This was followed by partial melting of the protolith during the late Paleozoic, which may have led to partial resorption of the zircons before continued zircon growth as the melt composition evolved. This event gave rise to the blue igneous rims present in some of the zircons and also led to significant Pb-loss in the older generation of zircons. Granulite facies metamorphism followed shortly thereafter, leading to development of the bright blue metamorphic rims found on some of the zircons.

Fig. 1. Images of zircons from the McBride lower crustal xenoliths: (a) PPL image of two zircons from mafic restite xenolith 83-159. Note lack of internal features. (b) CL and BSE images of the zircon in (a). The core and rim are revealed in both images, while dark areas in CL are bright in BSE. Note the three SHRIMP analysis pits. (c) CL image of zircons from metaadamellite xenolith 83-162. Igneous cores and metamorphic overgrowths are apparent in the zircons in the bottom row. Note the asymmetry of the cores relative to the whole zircons. Note also the left and right zircons in the middle row do not contain cores (see text). (d) CL image of zircons from mafic cumulate xenolith 85-107. Note the presence of igneous cores and metamorphic overgrowths, and the irregularity of the metamorphic rim thicknesses. (e) CL image of a zircon from metasedimentary granulite xenolith 83-157. Note the fractured core (dark green CL) with igneous growth zoning, surrounded by an outer core (lighter green CL), which is surrounded by a metamorphic overgrowth (blue-green CL) (f) CL image of a zircon from metasedimentary granulite xenolith 83-157. Note the round core which contains igneous growth zoning and the bright blue CL metamorphic overgrowth, and that the core zoning is truncated at the core–overgrowth boundary. (g) CL and BSE images of a zircon from mafic restite xenolith 83-159. An igneous core is revealed with both CL and BSE. However, the fine scale igneous growth zoning is only revealed in CL. Also, note the truncation of the igneous zoning at the core–rim boundary. (h) CL image of a group of zircons from mafic restite xenolith 83-159. Note the truncated igneous growth zoning in the core of the zircon at top center. Also note the variability of overgrowth thickness, and the asymmetry of cores with respect to the overgrowths. Field of view in (a) is 500 μm; (c) 660 μm; (d) 330 μm; (e) 200 μm; (f) 480 μm and (h) 770 μm.

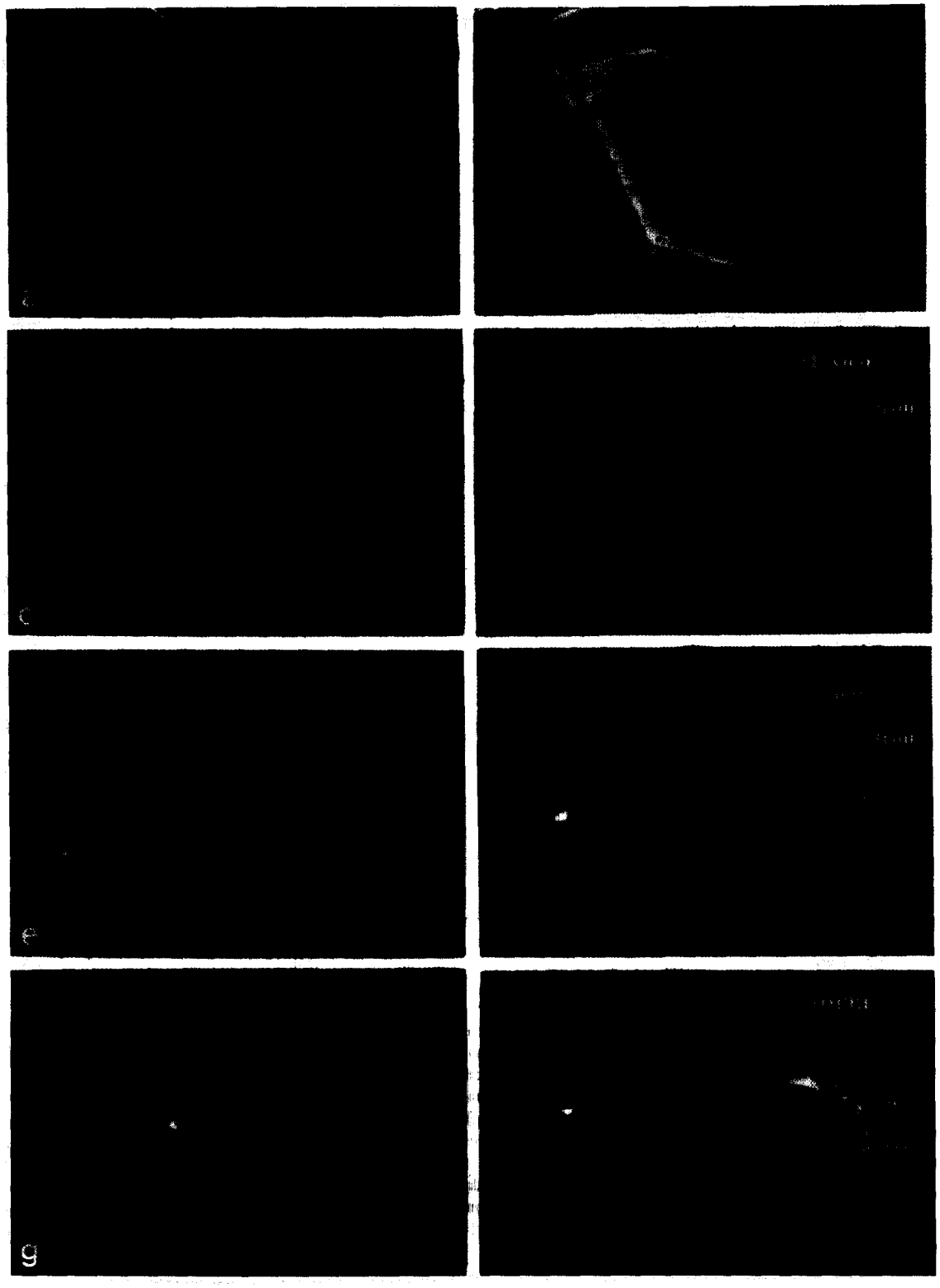
g

5.2. Summary of the McBride xenoliths

The zircons from the McBride xenoliths share one trait regardless of the intrasample variations we have discussed above: they all contain inherited igneous cores (revealing one or more periods of igneous growth) and metamorphic rims. The structures revealed by the CL imaging correspond nicely with the U–Pb ages obtained by Rudnick and Williams (1987) and with the regional geology (e.g., Rudnick and Taylor, 1987; Rudnick and Williams, 1987).

Most zircons from xenoliths 85-107 and 83-162 have cores that emit a dull gray to yellow CL, with metamorphic overgrowths that generally emit bright blue CL. Many of the cores contain inclusions of volatiles, glass, or minerals. The core and rims in these samples exhibit a spectrum of ages ranging between 200 and 340 Ma, reflecting igneous crystallization in the Carboniferous, followed by Permo-Triassic metamorphism.

The zircons from xenoliths 85-157 and 83-159 are unlike zircons from the other McBride xenoliths, these are also the only zircons to reveal any structure with BSE. In both 83-157 and 83-159 many of the zircons reveal very subtle core structures with a slightly brighter (higher mean "Z") BSE image than the outer regions of the grains. None of the BSE images reveal the fine-scale details seen in the CL images.

5.3. La Olivina xenoliths

Zircons from five xenoliths from La Olivina were investigated for this study, four of which are discussed below. Most of the zircons from La Olivina retain their original SHRIMP pits, so it is possible to determine the exact analysis locations (cf. Fig. 2).

Intermediate granulite MN-40. The zircons from this xenolith are pale orange and structureless in PPL, oval to elongate, and full of inclusions of granitic glass and apatite. U–Pb ages range from 25 to 37 Ma, except for one core, which yielded an age of 200 Ma (Rudnick and Cameron, 1991).

Many of these zircons exhibit pronounced igneous growth zoning when viewed with CL, and some show zoning with BSE; however, the resolution of detail is limited compared to CL (Fig. 2a and b). Four types of zircons can be identified with CL: (1) Zircons having two regions of yellow to blue CL igneous growth (i.e., an inherited core with igneous growth zoning surrounded by subsequent younger igneous growth) surrounded by a thin (10 μm thick) light blue CL metamorphic overgrowth. (2) Zircons similar to type 1 with only one region of igneous growth (lower zircon in Fig. 2a). (3) Zircons with two regions of igneous growth and no metamorphic overgrowth (upper zircon in Fig. 2a and single zircon in Fig. 2b). (4) Zircons that are structureless in CL and BSE revealing no core and rim relationships. The CL emission of the type 4 zircons is similar to others in the mount.

One zircon (#8, type 3 above) yielded a core $^{206}Pb/^{238}U$ age of 200 Ma, and a rim age of 37 Ma. Both of these growth zones (as well as the SHRIMP analysis pits) can be identified with BSE in Fig. 2b. None of the younger metamorphic rims in this sample were

Fig. 2. CL and BSE images of zircons from the La Olivina and the Newer Basalts xenoliths: (a) CL image of zircon #8 from La Olivina xenolith MN-40. Field of view is approximately 600 μm. CL reveals two regions of igneous growth zoning in this zircon. (b) BSE image of zircon in (a). Note that the two regions of igneous growth are revealed in BSE, however, the fine scale features are not. Note the two SHRIMP analysis pits in the BSE image (see text). Scale bar at upper right is 100 mμ. (c) CL and BSE images of zircon #15 from La Olivina xenolith MN-19. Note the complex core structures (see text) and the metamorphic overgrowth revealed in CL, and the lack of these features in BSE. Note the SHRIMP analysis pit in both the CL and BSE images. (d) CL and BSE images of zircon #11 from mafic granulite MN-19. We infer this zircon to consist solely of metamorphic growth. (see text). Note the lack of structure in BSE and CL. Note the SHRIMP analysis pit in both CL and BSE (e) CL and BSE images of zircon #14 from metapelite xenolith GNX-22. The igneous core and metamorphic overgrowth are visible with CL. A faint outline of the core is revealed in BSE, however, not to the degree as with CL. Note the SHRIMP analysis pit in the core of the zircon. (f) CL and BSE images of zircon #1 from intermediate granulite xenolith GNX-20. Note the difference in features revealed with CL and BSE. The filled paleo-fractures revealed in CL [white arrows point towards these features in (f) and (g)] are not seen in BSE. Note the three SHRIMP analysis pits in this zircon. (g) CL and BSE images of zircon #18 from intermediate granulite xenolith GNX-20. CL reveals a thin, quite variable in thickness, metamorphic rim. Note the one SHRIMP analysis pit. Similar to (f), BSE reveals little of the internal structure in this zircon. (h) CL and BSE images of zircon JMH-1 from the Newer Basalts xenolith 84-400. CL reveals complex internal structures in this zircon. BSE reveals the same features, although in much less detail. The imaging reveals that this zircon contains an altered core (white arrows point towards this feature), as well as three regions of subsequent zircon growth. (see text). Note the asymmetry of the core to the outer zircon growth, and the four SHRIMP II analysis pits.

dated with SHRIMP. We have identified other zircons in the mount, including some of those analyzed with SHRIMP, that may also contain inherited cores similar to #8, although the inherited cores were not analyzed. In those zircons only the outer igneous growth was dated. The granitic glass and apatite inclusions occur generally in equal proportions in both of the igneous growth regions and never in the metamorphic overgrowths. The type 4 zircons do not contain inclusions.

Intermediate granulite MN-19. The zircons from this xenolith are orange and round to elongate in PPL. SHRIMP analyses yielded a cluster of data within error of concordia between 360 and 160 Ma, with several other near-concordant analyses plotting at younger ages (down to 10 Ma).

Faint traces of internal structure are seen in BSE, whereas in CL these zircons reveal two distinct features: dull blue to gray, structureless cores, and light blue structureless overgrowths (Fig. 2c). None of these exhibit what we infer to be igneous growth zoning. Some of these zircons contain green patchy CL regions between the core and metamorphic overgrowth. The young ages ($^{206}Pb/^{238}U$ age = 2–40 Ma) determined by Rudnick and Cameron (1991) all occur within the light blue outer regions of the zircons, or within zircons that do not contain inherited cores, and are inferred to be composed entirely of young metamorphic growth (Fig. 2d). The dull blue to gray CL cores have a continuum of ages between 350 and 160 Ma (fig. 8c of Rudnick and Cameron, 1991) with no discernible difference in cores of different ages. A few of the zircons also contain inner bright gray cores, but these do not appear to be of age significance (e.g., the $^{206}Pb/^{238}U$ age of a bright gray core in zircon 15.1 is 251 ± 6 Ma).

It is interesting to note that although the Nd isotope model age for this xenolith suggests a Proterozoic source (Cameron et al., 1992), none of the cores imaged by CL or BSE and dated by SHRIMP are older than the 350 Ma. It possible that these cores exist; however, they are not distinguishable in CL or BSE images.

Metapelite GNX-22. The zircons from this sample are generally round and colorless in PPL and free of inclusions. SHRIMP analyses fall within error of concordia between 1000 and 15 Ma, with a clustering of data between 15 and 40 Ma (Rudnick and Cameron, 1991, Fig. 2).

In BSE these zircons reveal faint traces of cores, and in CL these zircons reveal three distinct populations: (1) Zircons with one or more inherited igneous cores having yellow to green CL, and thin (20 to 25 μm) dark to light blue metamorphic overgrowths (Fig. 2e); (2) Unzoned zircons that have the same CL color as the cores of the first type; (3) Unzoned blue CL zircons that have the same color as the metamorphic rims in the first type.

The Proterozoic and Paleozoic ages correspond to both the inherited igneous cores and whole zircons with similar yellow to green CL. The wide range in ages may reflect the diversity of the provenance from which the detrital zircons were derived. In contrast, the metamorphic overgrowths and the metamorphic zircons without cores all fall in the 10–40 Ma age range.

Intermediate granulite GNX-20. The zircons from this sample are colorless in transmitted light and range from round to very elongate. A few of the zircons contain inclusions of granitic glass and apatite. The SHRIMP analyses define two age populations: 1.37 Ga and 1.1 Ga; zircons from both of these populations suffered Pb-loss in the late Cenozoic (Rudnick and Cameron, 1991).

There is little internal structure revealed with BSE. However, using CL these zircons are very complex and heterogeneous. In general, these zircons have inherited igneous cores with light to dark blue CL, and thin (e.g., 20 μm) metamorphic overgrowths having bright blue CL. Regardless of the core and rim relationships, nearly all of the zircons from this xenolith have what we infer to be paleo-fracturing with subsequent fluid-assisted filling of the fractures (Fig. 2f and g). This feature is only observed in the cores and never extends into metamorphic overgrowths.

The two age populations of zircons in GNX-20 cannot be correlated to structures or colors revealed by CL. Most of the analyses from these two populations, as well as the younger Paleozoic ages, occur in both the dark and light blue CL core regions; no correlation between age and CL color is discernible within the cores. Many of the SHRIMP analyses are in close proximity to the fracture filled regions. However, these fractures occur in regions that include both of the Proterozoic ages as well as the younger Paleozoic ages (Fig. 2g). These filled fractures may indicate that the zircons were infiltrated with fluids from the surrounding environment, which may have facilitated Pb-loss.

The highly discordant ages recorded in the cores of these zircons may therefore be related to this alteration.

5.4. Summary of the La Olivina xenoliths

Zircons from each of the La Olivina lower crustal xenoliths are different, as are their crystallization ages. The zircons from four of the La Olivina xenoliths each contain distinctive internal structures when viewed with CL. Little structure is revealed in any of the La Olivina zircons with BSE, except in GNX-22 where an occasional core is revealed, and in MN-40 where the boundary between the inherited igneous cores and the younger igneous growth is revealed. MN-20 reveals no internal structure in PPL, CL or BSE.One feature that is shared by three of the xenoliths (GNX-20, GNX-22 and MN-19) is that they all contain zircons that have blue CL metamorphic overgrowths, as well as whole zircons that emit a similar blue CL and do not contain cores. These zircons yield Cenozoic metamorphic ages. The La Olivina zircons contrast greatly with the McBride zircons, which generally share similar structural and age relationships to one another.

5.5. The Newer Basalts xenolith

Metapelite 84-400. The zircons in this xenolith range in size from 60 to 100 μm. These zircons are clear, round, multifaceted crystals that reveal little internal structure in PPL. U–Pb SHRIMP II results are near-concordant and range from mid-Proterozoic to 150 Ma, preserving a record of both diverse provenance for the sedimentary protolith as well as younger metamorphic growth (King et al., 1993).

BSE reveals structure in only a few zircons, but CL reveals complex internal structures. Many of the zircons have cores surrounded by one, two, three, and in some cases four regions of subsequent zircon growth which emit green to yellow, or blue, CL. The cores generally have a high degree of asymmetry and occur near, or exposed at, the edge of the grain. The cores vary greatly in size, from 10 to 60 μm. A few of the cores have inner regions which we infer to be paleo-fractured with subsequent fluid-assisted filling of the fractures similar to La Olivina xenolith GNX-20 discussed above. These regions emit either a dark gray to pale green CL with the fractured regions emitting a brighter green to yellow CL (Fig. 2h). In many of the 84-400 zircons these inner core regions are surrounded by an outer core which is structureless and emits bright green to blue CL. In other zircons the cores are featureless and emit green CL. With these zircons there is usually, however, a distinct boundary between the core and subsequent overgrowth; each region has an unique CL emission.

In some cases it is difficult to make a distinction between core and rim growth. In general, besides having distinctive CL emission, the rims are more regular and symmetrical. Also, the filled fracture regions never extend beyond the core. Many of the cores appear to be fractured, angular fragments of formerly larger zircons, thus reflecting residence in a supracrustal environment following initial crystallization and before the next period of zircon growth (e.g., Hanchar and Miller, 1993). In this regard the zircons from this xenolith are similar to the McBride xenolith 83-157. This is in agreement with the interpretation by King et al. (1993) that this xenolith is a metasediment. In general, however, there is little evidence for igneous growth zoning in the cores of these zircons, so it is difficult to determine the degree of core fragmentation in all but a few zircons.

The youngest ages recorded in the 84-400 zircons are from the metamorphic rims, however, few spots lie entirely on the rims, so it is not clear that the most recent metamorphic event was dated. For example, zircon JMH-1 (Fig. 2h) reveals a wide range of ages and U concentrations. The apparently homogenous core ranges from 515 to 1100 Ma and has moderate U content, whereas the rim, whose age has not been well determined due to overlap of the SHRIMP II spot onto the core, has high U content and a younger (undetermined) age. It is also possible that the filled fractures seen in many of the 84-400 zircons are evidence of a disturbance of the isotope systematics.

6. Discussion

One aspect of our imaging results that is fundamentally important is that metamorphic overgrowths are unzoned and usually thin, on the order of 10 to 30 μm (however in some cases may be thicker). This observation is consistent with our previous investigation of zircons from other granulite facies lower crustal xenoliths and from granulite terranes (Hanchar and Miller,

unpubl. data), and was also noted by Zeitler and Williams (1988). Without CL and BSE imaging these rims could easily be overlooked and the age of metamorphism go undetermined. Moreover, the presence of these rims could also lead to mixed ages if the SHRIMP analysis straddles the rim and core of the zircon (cf. Zeitler et al., 1990). This may explain much of the scatter of data along concordia seen in the youngest zircons from McBride and La Olivina xenoliths. However, Pb loss is also demonstrated in these samples by core analyses that are strongly discordant (e.g., many of the analyses in 83-159 and GNX 20).

The relative constancy in metamorphic rim thicknesses (i.e., 10–30 μm), irrespective of the diameter of the core, suggests that the zircons all experienced a similar metamorphic growth rate (i.e., more zircon components are needed to grow a 30 μm thick rim on a 200 μm diameter core, than are needed to grow a 30 μm rim on a 100 μm diameter core). This suggests that zircon growth did not occur in a fixed reservoir, i.e., the Zr and Si were constantly being replenished, perhaps in the metamorphic fluid phase. It is likely that the position of the zircon within the rock will influence zircon growth during metamorphism. For example, zircons at grain boundaries may be more susceptible to exchange with fluids during metamorphism, resulting in more growth and possibly recording of younger ages compared to zircons trapped within minerals that are stable throughout the metamorphism (such as feldspar, or perhaps garnet).

It is interesting to note that zircons from both peraluminous granitic rocks and aluminous metasedimentary rocks, share a common trait of having thin rims. In our experience, zircon growth in peraluminous igneous rocks is manifested by either small acicular zircon needles, or thin igneous overgrowths on inherited cores (e.g., Miller et al., 1992; Hanchar and Miller, 1993). These observations are consistent with the low solubility of Zr in peraluminous melts (Watson and Harrison, 1983) and suggests a similarly low Zr solubility in metamorphic fluids associated with aluminous sediments.

We have demonstrated that most zircons from lower crustal xenoliths have multiple growth events preserved within them, none of which are visible with conventional microscopy techniques. It would therefore be difficult, if not impossible, to date the individual events recorded in these zircons by isotope dilution U/Pb geochronologic techniques. Even single-crystal analyses would suffer from the difficulty of isolating the thin metamorphic rims from the older cores. The zircons from xenolith 84-400 are a good example of this. These zircons are small (≤ 80 μm) and in some cases may record as many as five geologic events. In addition, the old cores are not always in the center of the grain (Fig. 3h) so abrasion would do little to unravel the history of these crystals.

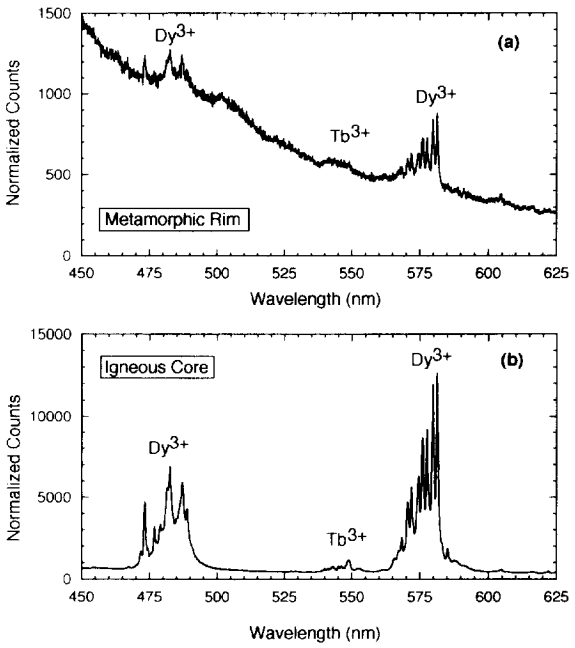

Fig. 3. CL emission spectra of the igneous core and metamorphic overgrowth region of the zircon shown in Fig 1g. The area in each region from which the spectra were collected is approximately 20 by 20 μm. Both spectra were collected under identical conditions and are normalized to the quantum efficiency of the CCD detector. (a) Most of the CL in the rim is a broad band blue to yellow emission, with a minor contribution from Dy^{3+} and Tb^{3+}. (b) In the core region, most of the CL emission is due primarily to Dy^{3+} with Tb^{3+} having a minor effect.

One needs to consider the motivation of a particular geochronologic study. If the goal of a particular study is only to constrain the age of crystallization of an inherited zircon core, then abrasion of zircon grains could be effective in removing the younger rim material (Tucker et al., 1989). This is, of course, at the expense of losing information on the younger geologic events preserved in the outer growth regions of the zircon. In other cases, it has been shown to be effective to break

off pieces of zircons (in some cases with subsequent abrasion of the fragments) and analyze the fragments by U/Pb isotope dilution techniques (e.g., Corfu et al., 1994). In either of these cases it would be useful to access the zircon population with CL and/or BSE to understand the complexity of the zircons being studied.

Can the structures revealed by CL and BSE be quantified in terms of trace element abundances? This is generally difficult because of secondary luminescence effects such as nonradiative energy transfer between, for example, Ho and Dy, the effects of which are not well understood (Marfunin, 1979; Roeder et al., 1987; Remond et al., 1992). Also, the outer electrons of the REEs, which are involved in the CL emission of natural zircons, are more influenced by their surroundings (i.e., neighboring electrons and nuclei) than their inner electrons, which are utilized in X-ray spectroscopy.

The CL emission spectra in Fig. 3 were collected from the metamorphic overgrowth and igneous core regions of the zircon in Fig. 1g. Both spectra were collected under identical conditions, and the areas sampled were approximately 20 by 20 μm in each region. Note the different scales of the y-axes. It is clear from these spectra that the CL intensity in the core is roughly 10 times that of the rim, suggesting a higher abundance of HREEs in the core compared to the rim. However, the peak intensities are not linear functions of concentrations (cf. Roeder et al., 1987). The core and rim of this zircon each have an unique CL "fingerprint", and these different "fingerprints" can be used to identify different periods of zircon growth contained within a given zircon.

An electron microprobe traverse across this zircon reveals that Hf concentration is a factor of ~ 1.3 higher in the core compared to the rim (Fig. 4). We attribute this to the igneous environment in which the core grew compared to the metamorphic environment in which the rim grew (i.e., in equilibrium with garnet). The data for Y, P, U and the HREEs also show similar core to rim variations, however, the error bars are larger and the trends are not as clear. Similar results have been reported in previous studies (cf. Zeitler et al., 1990; Hanchar and Miller, 1993). μPIXE (micro particle induced X-ray emission) analyses of the rim and core of this zircon (J.M. Hanchar and D.J. Cherniak, unpubl. data) reveal that although there are more heavy rare-earth elements (HREEs) in the core (by a factor of 2.3) than the rim, the order of magnitude variation

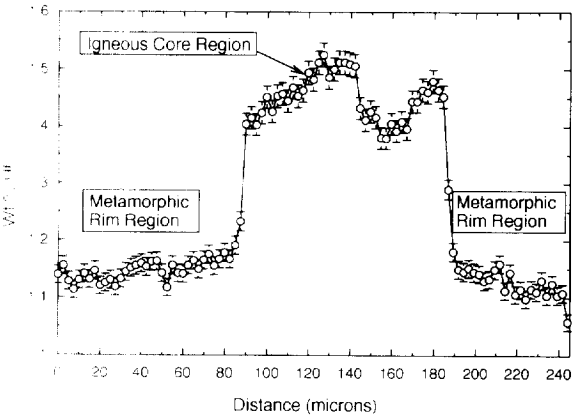

Fig. 4. Electron microprobe traverse across the zircon in Fig 1g. Wt % Hf is plotted against distance across the zircon. The error bars represent 1σ uncertainty. This figure demonstrates that the BSE-and CL-revealed structures can be correlated to variations in Hf concentrations, and that Hf concentrations vary considerably between the BSE- and CL- revealed igneous core and metamorphic overgrowth regions. Error bars represent 1σ errors from the counting statistics.

observed in the CL spectra is not present. Other blue rims on zircons from this same sample (e.g., Fig. 1b) do not show depletion of HREE and Hf and are therefore interpreted as igneous overgrowths.

It is our experience that the core–rim relationships illustrated in this paper are common in zircons from granulite facies terranes and xenoliths (J.M. Hanchar and C.F. Miller, unpubl. data). Usually there is a major change across the core–rim boundary that can be detected by BSE, or CL (including both changes in zoning and other internal structures and the color of the CL emission), or in some cases both techniques. Also, as noted above, the core–rim relationships can be verified by other microanalytical techniques (e.g., CL emission spectroscopy, electron microprobe, μPIXE, synchrotron X-ray fluorescence). Without CL and BSE imaging, however, these different regions within the zircons from granulite facies xenoliths would go undetected.

In many zircons from granulites the outermost rim in the zircon is unzoned, commonly emits a blue, yellow, or green CL, and is what we infer to be the most recent metamorphic growth (i.e., the metamorphic overgrowth or rim). There are examples of this from the McBride, La Olivina and the Newer Basalts zircons. There are also zircons from McBride and La Olivina that consist solely of unzoned zircon with blue CL, as

well as zircons with green to yellow CL that do not contain metamorphic rims. As noted above, the location of the zircon in the host rock may control whether or not a given zircon is affected by and records a given geologic event.

The colors of the CL emission of metamorphic rims are not unique to metamorphic growth; there are zircons from granitoid rocks that exhibit colors with similar CL emission spectra (J.M. Hanchar, unpubl. data). The differences in CL emission colors can be used to plan future, and interpret previous, ion probe studies. CL, in conjunction with BSE, can be used to unravel the complex histories of zircons. As noted above, zircons may contain information from multiple geologic events and detailed SHRIMP analyses, guided by CL and BSE imaging are required to identify all of the different geologic events.

7. Conclusions

(1) Zircons from lower crustal xenoliths commonly reveal little internal structure in PPL, reflected light microscopy, or by acid etching. This is inferred to be due to their residence in the hot lower crust where radiation damage is annealed out, rendering the zircon featureless with conventional microscopy.

(2) CL, and to a lesser extent BSE imaging reveals internal structures otherwise invisible. Both techniques usually reveal the same gross structures, with CL revealing fine-scale details. Different geologic events preserved in zircons generally have different internal structures (e.g., igneous growth zoning, metamorphic growth), and different color CL emissions. Sometimes these CL color variations can be directly correlated to age.

(3) Zircons from xenoliths from the three localities investigated here generally have igneous cores and thin metamorphic rims. Some zircons have two or more generations of growth within the cores and, in others, one or possibly more metamorphic overgrowths. In many cases there is a high degree of asymmetry in the core/rim relationships (i.e., the core might be near to the rim or exposed at the edge of the zircon). These features, coupled with the small zircons sizes (generally < 100 μm long) makes conventional U/Pb zircon analyses of these samples extremely difficult to interpret.

(4) Igneous cores and metamorphic rims commonly have distinctive CL emission spectra. These emission spectra may be used as a guide to identify different regions within a zircon, or homogeneity within a zircon population for planning ion probe studies. A linear relationship does not exist between CL intensity and trace element concentration in natural zircons. Therefore, the CL emission spectra can only be used as a qualitative tool in planning geochronologic studies.

(5) Igneous and metamorphic growth in zircons from lower crustal xenoliths, revealed with CL and BSE, can in some cases be correlated to Hf, Y, P, U and the HREEs concentrations in different growth zones.

Acknowledgements

This research was supported in part by NSF grants EAR-8904177, EAR-9205793, and EAR-9220095 to Bruce Watson. Thanks to Bruce Watson and Calvin Miller for encouraging the ideas presented in this paper, to Tony Mariano for discussions on cathodoluminescence, and to Daniele Cherniak, for reviewing an earlier version of this paper, and for help with the μPIXE analyses at SUNY–Albany. Penny King kindly permitted use of some of her unpublished results. Thanks to Ian Williams and Yadong Chen for their thorough review of this manuscript.

References

Black, L.P., Williams, I.S. and Comptston, W., 1984. Four zircon ages from one rock: the history of a 3,930 Ma-old granulite from Mount Somes, Enderby Land, Antarctica. Contrib. Mineral. Petrol., 94: 427–437.

Cameron, K.L., Robinson, J.V., Niemeyer, S., Nimz, G.J., Keuntz, D.C., Harmon, R.S., Bohlen, S.R. and Collerson, K.D., 1992. Contrasting styles of pre-Cenozoic and mid-Tertiary crustal evolution in northern Mexico: evidence from deep crustal xenoliths from La Olivina. J. Geophys. Res., 97: 17,353–17,376.

Cherniak, D.J., Hanchar, J.M. and Watson, E.B., 1993. Rare earth diffusion in zircon. Eos Trans. Am. Geophys. Union, 74: 651.

Corfu, F., Heaman, L.M. and Rogers, G., 1994. Polymetamorphic evolution of the Lewisian complex, NW Scotland, as recorded by U–Pb isotopic compositions of zircon, titanite, and rutile. Contrib. Mineral. Petrol., 117: 215–228.

Drake, M.J. and Weill, D.F., 1972. New rare earth element standards for electron microprobe analysis. Chem. Geol., 10: 179–181.

Hanchar, J.M. and Miller, C.F., 1993. Zircon zonation patterns as revealed by cathodoluminescence and back-scattered electron images: Implications for interpretation of complex crustal histories. Chem. Geol., 110: 1–13.

Heaman, L.M. and Parrish, R.R., 1991. U–Pb geochronology of accessory minerals. In: L.M. Heaman and J.N. Ludden (Editors), Applications of Radiogenic Isotope Systems to Problems in Geology. Mineral. Assoc. Canada, Toronto, 19: 59–102.

King, P.L., Rudnick, R.L. and Williams, I.S., 1993. Geochronology of a lower crustal xenolith from western Victoria, Australia: Mapping different crustal domains. EOS Trans. Am. Geophys. Union, 74: 577.

Koschek, G., 1993. Origin and significance of the SEM cathodoluminescence from zircon. J. Micros., 171: 223–232.

Krogh, T.E., 1993. High precision U–Pb ages for granulite metamorphism and deformation in the Archean Kapuskasing structural zone, Ontario: implications for structure and development of the lower crust. Earth Planet. Sci. Lett., 119: 1–18.

Le Bas, M.J. and Streckeisen, A.L., 1991. The IUGS systematics of igneous rocks. J. Geol. Soc. London, 148: 825–833.

Marfunin, A.S., 1979. Spectroscopy, Luminescence, and Radiation Centers in Minerals. (Translated from the Russian by V.V. Schiffer.) Springer, Berlin, 352 pp.

Mariano, A.N., 1978. The application of cathodoluminescence for carbonitite exploration and characterization. In: C.J. Braga (Editor), Proc. Int. Symp. Carbonitites, 1st, Pocos de Caldas, Minas Gerais, Brazil, June, 1976 Brasil Departmento Nacional da Produção Mineral, Brasilia, pp. 39–57.

Mariano, A.N., 1988. Some further geologic applications of cathodoluminescence. In: D.J. Marshall (Editor), Cathodoluminescence of Geologic Materials. Unwin Hyman, Boston, MA, pp. 94–123.

Mariano, A.N., 1989. Cathodoluminescence emission spectra of rare earth element activators in minerals. In: B.R. Lipin and G.A. McKay (Editors), Geochemistry and Mineralogy of Rare Earth Elements. Mineral. Soc. Am., Rev. Mineral., 21: 339–348.

Marshall, D., 1988. Cathodoluminescence of Geologic Materials. Unwin Hyman, Boston, MA, 146 pp.

Miller, C.F., Hanchar, J.M., Wooden, J.L., Bennett, V.C., Harrison, T.M., Wark, D.A. and Foster, D.A., 1992. Source region of a granite batholith: evidence from lower crustal xenoliths and inherited accessory minerals. Trans. R. Soc. Edinburgh Earth Sci., 83: 49–62.

Ohnenstetter, D., Cesbron, F., Remond, G., Caruba, R. and Claude, J.-M., 1991. Émissions de cathodoluminescence de deux populations de zircons naturels: téntative d'interpretation. C.R. Acad. Sci. Paris, 313: 641–647.

Ono, A., 1976. Chemistry and zoning of zircon from some Japanese granitic rocks. J. Jpn. Assoc. Min. Petrol. Econ. Geol., 71: 6–17.

Paterson, B.A., Stephens, W.E., Rogers, G., Williams, I.S., Hinton, R.W. and Herd, D.A., 1992. The nature of zircon inheritance in two granite plutons. Trans. R. Soc. Edinburgh Earth Sci., 83: 459–471.

Remond, G., Ohnenstetter, D., Claude, J.M., Caruba, C. and Roques-Carmes, C., 1990. Cathodoluminescence of minerals with particular analysis of rare-earth element bearing crystals. Scanning, 12: 113–114.

Remond, G., Cesbron, F., Chapoulie, R., Ohnenstetter, D., Roques-Carmes, C. and Schoverer, M., 1992. Cathodoluminescence applied to the microcharacterization of mineral materials: a present status in experimentation and interpretation. Scanning Microsc., 6: 23–68.

Roeder, P.L., MacArthur, D., Ma, X.-P., Palmer, G.R. and Mariano, A.N., 1987. Cathodoluminescence and microprobe study of rare-earth elements in apatite. Am. Mineral., 72: 801–811.

Rudnick, R.L., 1992. Xenoliths — samples of the lower continental crust. In: D.M. Fountain, R.J. Arculus and R.W. Kay (Editors), The Continental Crust. Elsevier, New York, pp. 269–316.

Rudnick, R.L. and Taylor, S.R., 1987. The composition and petrogenesis of the lower crust: A xenolith study. J. Geophys. Res., 92: 13,981–14,005.

Rudnick, R.L. and Williams, I.S., 1987. Dating the lower crust by ion microprobe. Earth Planet. Sci. Lett., 85: 145–161.

Rudnick, R.L. and Cameron, K.L., 1991. Age diversity of the deep crust in northern Mexico. Geology, 19: 1197–1200.

Sommerauer, J., 1974. Trace element distribution patterns and the mineralogical stability of zircon — an application for combined electron microprobe techniques. Electron Microsc. Soc. S. Afr., Proc 4:, 71–72.

Sommerauer, J., 1976. Die Chemisch–Physikalische Stabilität Natülicher Zirkone und ihr U–(Th)–Pb System. Ph.D. Thesis 5755, ETH, Zürich, 151 pp.

Tucker, R.D., Krogh, T.E. and Råheim, A., 1989. Proterozoic evolution and age–province boundaries in the central part of the Western Gneiss Region, Norway: results of U–Pb dating of accessory minerals from Trondheimsfjord to Geiranger. In: C.F. Gower, T. Rivers and B. Ryan (Editors), Mid-Proterozoic Laurentia–Baltica. Geol. Assoc. Canada, Spec. Pap., 38: 149–173.

Vocke, R.D., Jr and Hanson, G.N., 1981. U–Pb zircon ages and petrogenetic implications for two basement units from Victoria valley, Antarctica. In: L. McGinnis (Editor), Dry Valley Drilling Project. Antarctica Research Series. AGU, Washington, DC, Vol. 33, pp. 247–255.

Watson, E.B. and Harrison, T.M., 1983. Zircon saturation revisited: temperature and composition effects in a variety of crustal magma types. Earth Planet. Sci. Lett., 64: 295–304.

Williams, I.S. and Claesson, S., 1987. Isotopic evidence for the Precambrian provenance and Caledonian metamorphism of high grade paragneisses from the Seve Nappes, Scandinavian Caledonides. Contrib. Mineral. Petrol., 97: 205–217.

Yang, B., Luff, B.J. and Townsend, P.D., 1992. Cathodoluminescence of natural zircons. J. Phys. Condens. Matter, 4: 5617–5624.

Zeitler, P.K. and Williams, I.S., 1988. U–Pb dating of metamorphic overgrowths by means of depth profiling with an ion microprobe. EOS Trans. Am. Geophys. Union, 69: 464.

Zeitler, P.K., Barreiro, B., Chamberlin, C.P. and Rumble, III, D., 1990. Ion-microprobe dating of zircon from quartz–graphite veins at the Bristol, New Hampshire, metamorphic hot spot. Geology, 18: 626–629.